



Kent Academic Repository

Alesbrook, L.S., Burchell, Mark J., Cornwell, L.T., Corsaro, R.D., Giovane, F., Liou, J.-C., Tandy, J.D. and Wozniakiewicz, P.J. (2024) *Hypervelocity impact induced light flash experiments on single and dual layer Kapton targets to develop a time of flight space dust and debris detector*. *International Journal of Impact Engineering*, 187 . ISSN 0734-743X.

Downloaded from

<https://kar.kent.ac.uk/104841/> The University of Kent's Academic Repository KAR

The version of record is available from

<https://doi.org/10.1016/j.ijimpeng.2024.104897>

This document version

Publisher pdf

DOI for this version

Licence for this version

CC BY (Attribution)

Additional information

For the purpose of open access, the author(s) has applied a Creative Commons Attribution (CC BY) licence to any Author Accepted Manuscript version arising

Versions of research works

Versions of Record

If this version is the version of record, it is the same as the published version available on the publisher's web site. Cite as the published version.

Author Accepted Manuscripts

If this document is identified as the Author Accepted Manuscript it is the version after peer review but before type setting, copy editing or publisher branding. Cite as Surname, Initial. (Year) 'Title of article'. To be published in **Title of Journal** , Volume and issue numbers [peer-reviewed accepted version]. Available at: DOI or URL (Accessed: date).

Enquiries

If you have questions about this document contact ResearchSupport@kent.ac.uk. Please include the URL of the record in KAR. If you believe that your, or a third party's rights have been compromised through this document please see our [Take Down policy](https://www.kent.ac.uk/guides/kar-the-kent-academic-repository#policies) (available from <https://www.kent.ac.uk/guides/kar-the-kent-academic-repository#policies>).



Hypervelocity impact induced light flash experiments on single and dual layer Kapton targets to develop a time of flight space dust and debris detector

L.S. Alesbrook^a, M.J. Burchell^{a,*}, L.T. Cornwell^a, R.D. Corsaro^b, F. Giovane^c, J.-C. Liou^d, J. Tandy^e, P.J. Wozniakiewicz^{a,*}

^a Centre for Astrophysics and Planetary Science, School of Physics and Astronomy, University of Kent, Canterbury CT2 7NH, United Kingdom

^b AstroAcoustics, 201 De La Gaye Pt, Beaufort, SC 29902, United States

^c Giovane Consultants, 576 Glebe View Lane, Lottsburg, Virginia 22511, United States

^d NASA Orbital Debris Program Office, NASA Johnson Space Center, Houston, Texas 77058, United States

^e Centre for Astrophysics and Planetary Science, School of Chemistry and Forensic Science, University of Kent, Canterbury CT2 7NH, United Kingdom

ARTICLE INFO

Keywords:

Hypervelocity
Light-flash
Kapton
Orbital debris
Impact speed
Time of flight

ABSTRACT

The impact flash from hypervelocity impact on thin (12.5 μm) Kapton film was observed. The projectile sizes ranged from 0.1 to 1 mm, with speeds from 2 to 5 km s^{-1} and penetrated the Kapton intact, leaving holes the same size as the projectile (to within measurement errors). The flash intensity (normalised to impactor mass) scaled with impact speed to the power 5.5. However, the data also suggest that at constant speed the intensity scales with the area of the hole in the Kapton and not the projectile mass (i.e. with some property of the target and not as a function of the projectile energy or momentum). Using two layers of Kapton, it was possible to construct a Time of Flight (TOF) system, which used the time of the onset of the flash in each layer to produce flight speeds accurate to within typically 1%. When compared to the projectile speed pre-impact, there was no indication of projectile deceleration during passage through the Kapton film. In addition, when PVDF acoustic sensors were placed on the Kapton film, they exhibited an electromagnetic “pick-up” signal from the impact of projectile on the Kapton, confirming suspicions of signal interference from past work with acoustic sensors. The ability of the light flash to provide accurate impact timing signals suggests the TOF system would be suitable for use as a cosmic dust or debris impact detector in space (e.g. Low Earth Orbit).

1. Introduction

Hypervelocity impacts are high-speed impacts that occur naturally in space as a result of the relative orbital speeds of objects around the Sun or local bodies (e.g. planets and moons), see [1], for a review. The impact speed is often in units of km s^{-1} , which can exceed the speed of the resultant compressive and tensile waves in the materials involved, generating stresses which exceed the strength of the materials. This causes them to behave as if strength-less during the early phases of an impact. As a convenient boundary, impacts at speeds above 1–2 km s^{-1} are usually considered hypervelocity. As well as behaving as if strength-less, hypervelocity impacts can involve melting and vapourisation of the materials involved, and can also generate an impact-related light flash.

This light flash phenomenon has been reported since early on in studies of hypervelocity impacts (e.g. [2]). It is an electro-magnetic emission across a range of wavelengths including the visual. Reports on the phenomena appear regularly in the literature, focussed on different aspects of the flash and applications thereof. At high speeds (order 20 km s^{-1}), the presence of a flash as an indicator of an impact, has long been proposed as a way to detect impacts of space vehicles on the lunar surface (e.g. see [3]). Indeed, even though at a slower speed of $\sim 2 \text{ km s}^{-1}$, the impact of the ESA’s Smart 1 spacecraft on the Moon [4,5] was observed by this method [6,7]. Impact flash was also eventually successful in detecting meteorites hitting the Moon [8] and is now a standard method for obtaining the meteorite flux on the Moon (e.g., [9, 10]).

There have been many reports of light flash from laboratory

* Corresponding authors.

E-mail addresses: m.j.burchell@kent.ac.uk (M.J. Burchell), p.j.wozniakiewicz@kent.ac.uk (P.J. Wozniakiewicz).

<https://doi.org/10.1016/j.ijimpeng.2024.104897>

Available online 23 January 2024

0734-743X/© 2024 The Author(s). Published by Elsevier Ltd. This is an open access article under the CC BY license (<http://creativecommons.org/licenses/by/4.0/>).

Table 1

Summary of shots. All speeds are from the gun velocity measurement system. The shot programmes define the target layout (see main text and Fig. 1 for details). PVDF sensors were present in programmes B and C. Of the 18 shots, 13 produced usable data.

Shot Programme	Shot	Speed (km s ⁻¹)	Projectile diameter (mm) and type	Projectile density (kg m ⁻³)	Comment
A	1	5.23	1.0 mm st 420	7800	Good
A	2	4.89	0.5 mm st 304	7930	Good
A	3	4.98	0.1 mm st 304	7930	Good
B	4	4.92	0.8 mm st 420	7800	Good
B	5	5.16	0.5 mm st 304	7930	Good
B	6	–	0.1 mm st 304	7930	Projectile didn't reach the target
B	7	–	0.3 mm st 304	7930	Projectile didn't reach the target
B	8	5.13	0.3 mm st 304	7930	Good
B	9	–	0.5 mm st 304	7930	Projectile didn't reach the target
B	10	3.82	0.5 mm st 304	7930	Good
B	11	2.00	0.5 mm st 304	7930	Good
B	12	4.94	0.5 mm st 304	7930	Good
B	13	4.89	0.5 mm st 304	7930	Good
C	14	–	1 mm st 420	7800	Projectile didn't reach the target
C	15	4.16	1 mm st 420	7800	Good
C	16	2.13	1 mm Titania	4510	O-ring failed, lots of debris hit Kapton
C	17	3.87	1 mm Titania	4510	Good
C	18	4.11	1 mm Aluminium	2710	Good

experiments involving mm sized projectiles at speeds of typically 2 – 6 km s⁻¹ impacting thick (i.e. effectively semi-infinite) solid targets such as rocks (e.g. [3,11]) and metals (e.g. [12]), powdered rock (e.g. [13]), metal plates (e.g. [14,15]), ices (e.g. [16]), etc. The impact flash can also be used to measure temperatures (e.g., [17]), and to look at fine structure in the flash to identify the plume constituents, study their time evolution and conduct spectroscopy [18–26], etc.

In parallel, impact flash from sub-micron particles hitting various surfaces such as metal [27–29] and ice [30] has also been reported. The light flash from sub-micron impacts has indeed been used in dust detectors in space to accurately flag the time of the impact, e.g., the PIA instrument [31] mounted on the Giotto spacecraft which flew past Halley's comet in the 1980s [32]. In this case, accurate determination of the impact time was important for time of flight (TOF) mass spectrometry conducted on the ionised contents of the plasma plume produced in an impact.

Since the early days of space-flight the hazard to space vehicles due to natural cosmic dust has been known and studied (e.g. see [33], for a recent review). However, spacecraft and their launch vehicles are a source of small particle debris in space, and, in recent years, one of the growing issues in sustainable use of space, has been the risk of impact on space vehicles in Earth orbit due to debris from human activities in space. Indeed, as use of space increases, this debris flux is an ever rising one. This is particularly an issue in low Earth orbit (LEO, e.g. see [34], or [35]), where, for some years now, it has been recognised that if the density of debris sources increases, a multiplicative runaway cascade event can potentially then occur generating more and more debris. This so-called Kessler syndrome can arise because impact on another object by a single piece of debris may, under certain conditions, result in generation of more debris, which can then in turn go on to impact more objects, generating more debris etc. (see [36]).

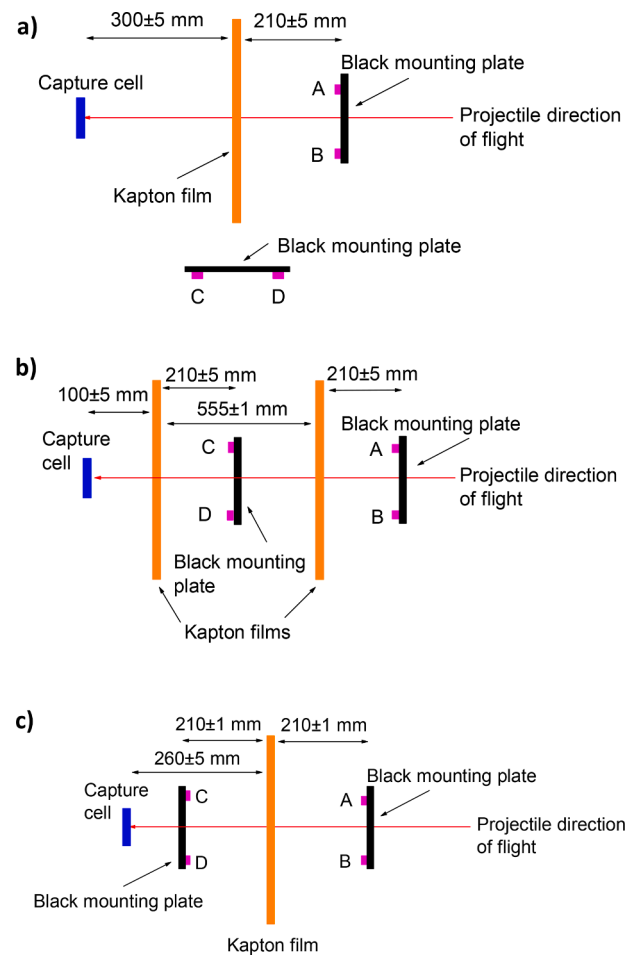


Fig. 1. Diagram (not to scale) showing set-up of detectors. (a) Programme A (shots 1 – 3). The black mounting plates hold the photodiodes (labelled A, B, C and D). A and B look directly at the front of the Kapton film, whereas C and D look sideways at the wall of the target chamber to detect any reflected light. (b) Programme B (shots 4 – 14). A and B look directly at the front of the first Kapton film, whereas C and D look directly at the front of the second Kapton film. (c) Programme C (shots 14 – 18). The black mounting plates hold the photodiodes (labelled A, B, C and D). In this set up, A and B look directly at the front of the Kapton film, whereas C and D look directly at the rear of the Kapton film. (Note that in all cases the black mounting plates had a central hole, (diameter 3.5 cm, to permit passage of the projectile).

The damage caused to space vehicles by the impact of mm and cm sized objects has long been studied. For example, in the 2010's, NASA conducted the DebrisSat experiment to see how impact by a cm sized object can disrupt a whole satellite and produce a new source of further debris [37]. However, the current flux of mm - cm sized objects in LEO is uncertain. It cannot be observed optically or tracked by radar from the ground (the most powerful radar systems can report the presence of, but not track, objects down to 3 mm size in LEO), and fortunately at present it is still low enough to require a large area detector operational for several years to measure it in-situ.

There have been attempts to measure the flux in the mm size range in LEO in-situ. In the 1980s, the NASA LDEF mission involved retrieving a satellite after 5.7 years in orbit (using the space shuttle Columbia) and much of its surface was scanned for impact features (e.g. see [38], or [39]). Similarly, in the 1990s and early 2000s, solar panels and radiator plates were retrieved from the Hubble Space Telescope and brought back to Earth (again by the space shuttle) and their surfaces studied for impact features (e.g. [40–42]). Indeed, even the windows of the shuttle itself were regularly examined for impact features, helping to provide flux measurements.

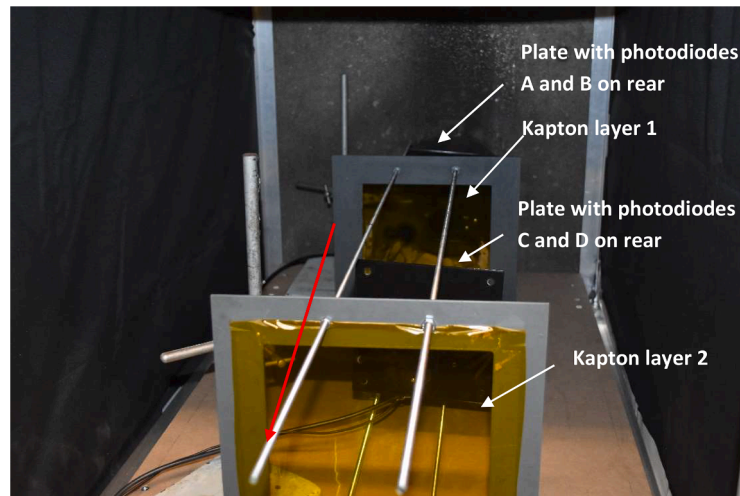


Fig. 2. Typical view of the detector in the target chamber (here the two layer Kapton target from Programme B, see Fig. 1b for dimensions) as seen from the rear. The second mounting plate with photodiodes positioned on its rear face is clearly visible, but the first plate is mostly hidden by the first Kapton layer. The direction of travel of the projectile is shown with a red arrow. The detector sits in a hollow box lined with black non-reflective curtains on the top and sides. The ends are open to permit entrance and egress of the projectile.

However, the retirement of the space shuttle fleet has meant that such activities no longer occur. Instead in the 2010s, NASA developed and deployed on the exterior of the International Space Station (ISS) as an exploratory technology demonstration, a large area (1 m^2) impact detector called DRAGONS/Space Dust System (SDS, see [43–45]). The SDS was a three-layer device, with a thin ($25 \mu\text{m}$) Kapton front face, which mm objects would penetrate, and a second Kapton film (again $25 \mu\text{m}$ thick and 150 mm behind the first layer) immediately followed by a metal plate to capture the penetrating particles. The two layers of Kapton in the SDS would thus act as a TOF detector giving impact speed. Use of acoustic sensors on all three layers (e.g. [46]), along with resistive grids on the Kapton films (e.g. [44,47,48]), would allow identification in real-time of the impacts and their location, thus permitting a direction of flight to be found. This direction, combined with the known pointing history of the ISS and the impact speed, was intended to permit an orbital determination for the impactor, assisting in its categorisation as orbital debris or cosmic dust. Calibration studies of the SDS showed that impact location could be found to within 0.8 cm , and impact speed for 0.2 to 1 mm diameter projectiles was accurate to $\pm 18\%$ [44]. Associated modelling of the then currently estimated flux, suggested the SDS would provide improved flux measurements for particles up to 0.2 mm in size in just 1 year, but for 1 mm objects a 10 year mission would be required to detect a single impact [44].

Unfortunately, the SDS failed after less than 1 month of operations (see [49] for a discussion). During this time it did show that impacts on the front layer could be detected, but even with a 1 m^2 exposed area, the flux for larger particles (typically $> 100 \mu\text{m}$) was too small to permit any penetrations of the front film with an associated impact on the rear layers.

One of the questions about the SDS TOF detection method, is whether or not the penetration of the front film significantly decreases the speed of the impactor. This would mean that the measured TOF speed is lower than the pre-impact speed. At small impactor sizes, deceleration will certainly occur. Indeed, at the smallest sizes there will be a size regime where there is no penetration, then as projectile size increases there will be penetration but disruption of the projectile, then intact penetration accompanied by deceleration, and finally intact penetration and no deceleration. But in which regime does the SDS operate? A recent paper [50] has shown that for stainless steel projectiles of 1 mm diameter impacting a two layer Kapton target at 2 and 4 km s^{-1} , there is no appreciable deceleration when penetrating the front Kapton layer. The resulting speeds measured using polyvinylidene

difluoride (PVDF) acoustic sensors (similar to those on the SDS) on the two layers were within 1% of the pre-impact speed. This is significantly better than the accuracy reported by [44], with the only significant difference being the thickness of the Kapton films ($12.5 \mu\text{m}$ in [50], vs. $25 \mu\text{m}$ in [44]). It is not known, however, what happens to smaller projectiles.

It was also suggested by [49] (from real data from the SDS) and by [50] (in laboratory experiments), that the start of the acoustic signals on the PVDF sensors can be preceded by a signal which was coincident in time across all sensors. It was suggested by both set of authors that this signal could represent some form of electromagnetic (EM) pick-up by the sensors of the light flash from the impact on the Kapton.

In this current paper, we thus first look specifically at the light flash from impacts on a $12.5 \mu\text{m}$ thick Kapton film, using photodiodes to detect the flash. Then we use two layers of Kapton (similar to the arrangement in the SDS and that used by [50]), utilising the impact flash on each layer to obtain a TOF speed between the two layers for a range of projectile sizes and speeds. Finally we vary the projectile composition at a fixed size and impact speed, to see how this influences the flash. We also use data from PVDF sensors to determine if the EM pulse accompanying the flash can be picked-up by “acoustic” sensors.

2. Experimental method

The experiments were performed using the two-stage light gas at the Univ. of Kent [51,52]. This can fire single projectiles into a large vacuum chamber, held at between approximately 0.25 and 0.5 mbar during a shot. The projectiles are initially carried in an isoplast sabot which is discarded in flight. The projectile speed is measured in flight in the gun by a variety of methods. The most accurate method is via passage of the projectile across two laser light curtains with a known separation ($499 \pm 1 \text{ mm}$) between them. These laser curtains are each focussed onto a photodiode read out by a fast digital oscilloscope at 400 MHz . For $0.2 - 1 \text{ mm}$ sized projectiles the obscuration of the laser light produces a sufficiently strong change in photodiode output to measure the projectile speed to within 1% . For smaller projectiles a second system is used which uses the exit of the sabot from the launch tube to give a first time point, followed by the impact of the sabot parts on a stop plate part way along the range of the gun to give a second timing point. For 0.1 mm diameter projectiles, this provides a speed estimate which is accurate to within $\pm 5\%$.

The targets were sheets of $12.5 \mu\text{m}$ thick Kapton, mounted onto

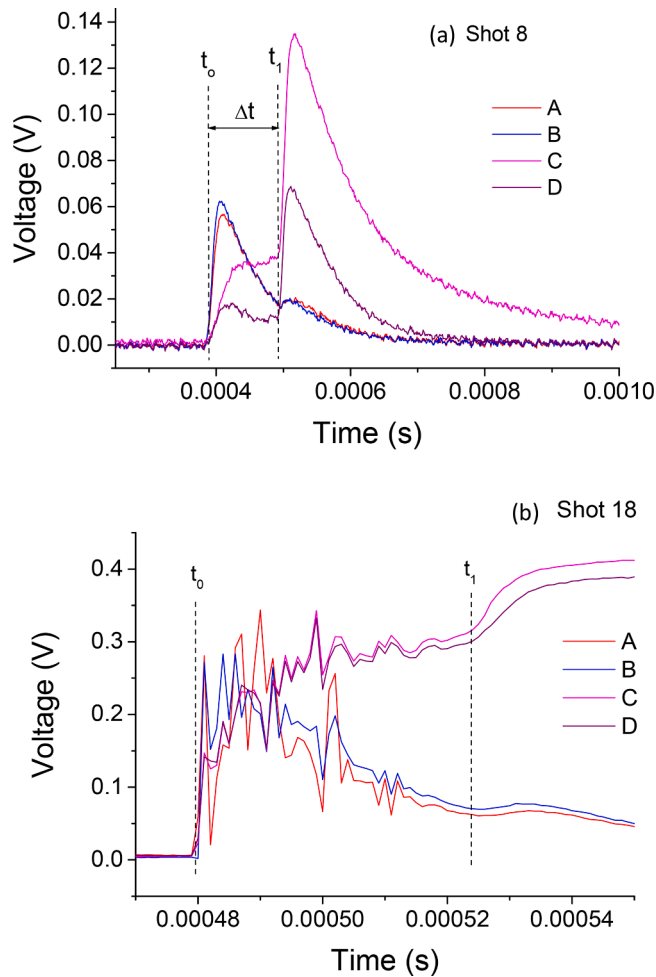


Fig. 3. Example photodiode data vs time. (a) Shot 8, typical of programmes A and B, where the signals in the raw data were $-ve$ going in amplitude, but here have been baseline subtracted and inverted for ease of display. Starting at t_0 , the front photodiode signals (A&B) initially rise sharply, and peak some 10 - 15 μ s later before falling back. Then at t_1 there is a second rise to a smaller second peak due to the flash from the impact on the second layer of Kapton. The second layer of photodiodes (C and D) rise a little when A and B start (i.e. they see the front flash) and then fall slightly, before rising more sharply at t_1 when the impact occurs on the second Kapton layer. (b) Shot 18, typical of programme C. The photodiode signals are now $+ve$ going in amplitude and show fine structure in the first 30 μ s. All photodiodes are looking at a single layer of Kapton (A and B at the front of the Kapton, and C and D the rear). The signals rise to an initial maximum in some 10 μ s (as in earlier shots). A and B then decline, while C and D remain at the maximum. There is then a later rise in all signals at t_1 . This occurs in all shots in programme C and is some 40 - 45 μ s after the impact on the Kapton.

plastic frames. The sheets came in two sizes, either 25 cm \times 25 cm, or 15 cm \times 15 cm. The frames carrying the Kapton were mounted on metal rods to separate the multiple layers by a known distance, and keep the films at normal incidence to the projectile direction of flight.

The projectiles used in this work were mostly stainless steel (herein st) spheres (st grade 304 or 420, of density 7930 and 7800 kg m^{-3} respectively) of diameter (d) 0.1 to 1.0 mm (the diameters are accurate to typically 1.5% or less). When combined with a Kapton thickness (f) of 12.5 μm , this gives an f/d range of 1/8 to 1/80. Two grades of stainless steel were used, as the full range of sizes was not available in the laboratory with a single grade. In two shots, 1 mm diameter spheres of titania (titanium oxide) and aluminium were used.

In all shots, a projectile capture system was placed behind the target. This had several layers of thick paper card followed by two layers of 3

mm thick aluminium plates. The intention was to permit the projectile to pass through the card layers and then stop it via an impact on the metal back-plate. Any ejecta from the crater in the metal would likely be captured by the card and not spray backwards onto the rear of the Kapton targets.

The photodiodes were BPW 34, PIN Si photodiodes, made by Vishay (for details see <https://docs.rs-online.com/220c/0900766b80de9fc5.pdf>). They were mounted onto 3D printed black plastic sheets (to prevent reflections) which were fixed to backing sheets of aluminium. The black surface always faced the Kapton surface the photodiodes were looking at. Photodiode readout was via pre-amps (type CA3140EZ) into a data-acquisition system operating at 1 MHz, with 3000 data points per photodiode per event. The system was triggered by the impact of the sabot sections on the stop plate in the gun.

In a few shots, three PVDF acoustic sensors (type TE-FTD1-028 K) were also used (the same type as in [43,50]). These were attached to the Kapton film using adhesive. Two had an active area of 22.5 mm^2 and were mounted on the front and rear face of a Kapton layer. The third had an active area of 45 mm^2 and was mounted onto the rear of the frame holding the Kapton. They were read-out via the same system as the photodiodes, but without the pre-amplification stage.

Three shot programmes were carried out (A, B and C) with a total of 18 shots (see Table 1). In four of the shots, the projectile did not travel down the gun and hit the target. This was mostly correlated with small projectiles, which travelled slightly off-axis and hit the stop plate (which was present to intercept the sabot). In one shot, an O-ring failed on the piston in the gun. The piston is driven by the detonation of the shot-gun cartridge, and compresses the light gas used to drive the sabot. When the piston O-ring failed, the shot still launched a projectile to the target, but at a slower speed than planned and it was accompanied by a cloud of debris which tore the Kapton film and made interpretation of the data impossible.

Each of the three shot programmes focussed on a different goal. Programme A (three good shots) was to establish if the light flash could be observed from impact on a single Kapton film, and establish what, if any, reflection was present from the target chamber walls. The shots were at a nominal impact speed of $\sim 5 \text{ km s}^{-1}$, with a range of projectile sizes. The set-up of the Kapton film layer and the photodiodes is shown in Fig. 1a. The Kapton film had the 25 cm \times 25 cm exposed surface area.

Programme B (6 good shots) was to determine if separate light flashes could be observed from a dual-layer Kapton target and a TOF (and hence speed) determined over a range of incident speeds and projectile sizes. The set-up of the dual-layer Kapton target and the photodiodes is shown in Fig. 1b, with a photograph in Fig. 2. PVDF sensors were mounted on the second (rear) Kapton layer in these shots. Both layers of Kapton had a 25 cm \times 25 cm exposed surface area.

Programme C was to determine how the light flash from a single layer depended on projectile mass (or composition) at a fixed impact speed ($\sim 4 \text{ km s}^{-1}$) and projectile size (1 mm). This used stainless steel 420 (density 7800 kg m^{-3}), titania (density 4510 kg m^{-3}) and aluminium (2710 kg m^{-3}). The detector set-up is shown schematically in Fig. 1c. The Kapton film had a 15 cm \times 15 cm exposed surface area. In programme C, the plates bearing the photodiodes were mounted on the same rods as the Kapton films to provide extra confidence in the relative spacing and reduce any variations in viewing geometry.

Examples of the photodiode output are shown in Fig. 3. Unfortunately, due to what was eventually identified as a floating earth issue in a power supply, the nature of the photodiode output changed over the course of the experimental programme. In programmes A and B, the signals were negative going in amplitude as flash intensity increased (with relatively short rise times, but longer decay times of variable duration, see Fig. 3a), whereas in C they were positive going (again with short rise times and moderate decay times, see Fig. 3b). However, this did not affect the ability to determine the onset time of the flash signals. Furthermore, in terms of signal intensity, no data from programmes A and B ($-ve$ signals) were used in the analysis of programme C ($+ve$

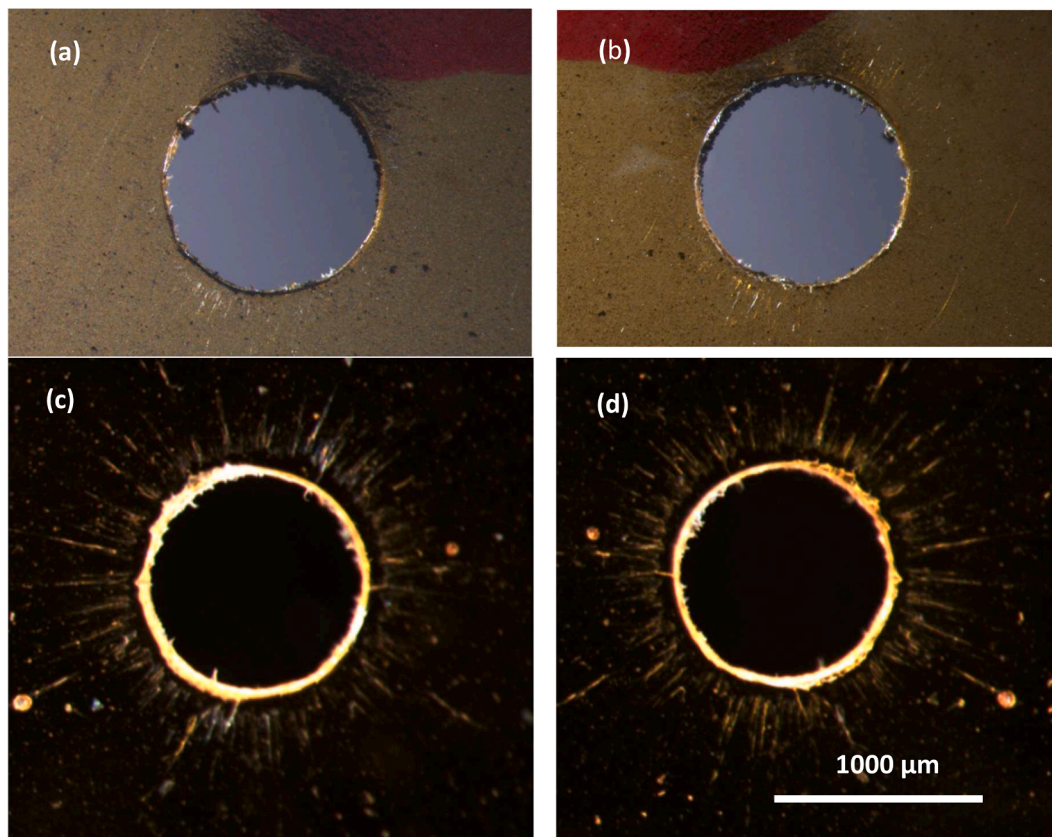


Fig. 4. Holes in Kapton layers. (a) and (b) are front and rear views of the hole in the single Kapton layer in shot 17. (c) and (d) are front and rear views of the hole in the second Kapton layer in shot 10. (c) and (d) have stronger lighting to show more clearly the melted rim around the hole along with the radial striations on the surface of the Kapton.

Table 2

The (background subtracted) intensity (I) of the light flash seen on each photodiode is given, along with the associated uncertainty in the next column. An entry of “sat” indicates that the photodiode saturated and the true peak intensity was not observed. The signals for photodiodes A and B in shot 4 just saturated and the values given here (marked with an *) are extrapolations (the extrapolation method is described in main text).

Shot	Speed (km s ⁻¹)	Projectile Diameter (mm)	Kinetic Energy (J)	I_A (V)	Δ (V)	I_B (V)	Δ (V)	I_C (V)	Δ (V)	I_D (V)	Δ (V)
1	5.234	1	55.94	sat.	–	sat.	–	0.3655	0.0007	0.4340	0.0007
2	4.868	0.5	6.150	0.3235	0.0007	0.223	0.0007	0.0575	0.0007	0.0730	0.0007
3	4.980	0.1	0.05149	0.1377	0.0007	0.0942	0.0007	0.0800	0.0007	0.1150	0.0007
4	4.925	0.8	25.36	0.83*	0.03*	0.77*	0.02*	0.5140	0.0007	0.3970	0.0007
5	5.157	0.5	6.902	0.6645	0.0007	0.6392	0.0007	1.1667	0.0011	1.2220	0.0011
8	5.131	0.3	1.476	0.0570	0.0007	0.0630	0.0007	0.0970	0.0007	0.0560	0.0007
10	3.816	0.5	3.779	0.0647	0.0007	0.0760	0.0007	0.1835	0.0011	0.1805	0.0011
11	2.000	0.5	1.038	0.0150	0.0011	0.0160	0.0011	0.0080	0.0011	0.0085	0.0011
12	4.941	0.5	6.336	0.3175	0.0011	0.3519	0.0011	0.2740	0.0011	0.2595	0.0011
13	4.892	0.5	6.210	0.4846	0.0007	0.5125	0.0007	0.2740	0.0007	0.2595	0.0011
15	4.158	1	35.30	0.3175	0.0007	0.2310	0.0011	0.3155	0.0007	0.3170	0.0007
17	3.846	1	17.46	0.3208	0.0007	0.2493	0.0007	0.3180	0.0007	0.2650	0.0007
18	4.109	1	11.98	0.3366	0.0011	0.2801	0.0007	0.3386	0.0011	0.3279	0.0011

signals) or vice-versa. Thus the analysis conditions were stable inside each programme.

In the examples of photodiode outputs shown in Fig. 3, the time of the onset of the flash is marked as t_0 . The flash intensity then increases to a maximum, typically some 10 μ s later (c.f. [24], report a rise time of 6 μ s for impacts on aluminium, and [15] report a peak after 2 – 3 μ s, again for impacts on aluminium). The photodiode intrinsic rise time is of order 100 ns, so the observed rise time is associated with the evolution of the flash itself.

Other structure can also be seen in the examples in Fig. 3. In Fig. 3a, the photodiodes looking at the second Kapton layer respond immediately the first layer is hit, indicating that some light reached them despite the shielding and blackout materials on the walls of the target

chamber. In some shots, it is also possible to observe a small signal when the projectile hits the capture cell down-stream of the target (when combined with the projectile speed, the time delay to these latter signals matches that expected from the known physical separation of the detector components given in Fig. 1). In shots 14 – 18 (programme C), two new effects were observed in the data as well as the change from negative to positive amplitude signals. First, the data showed fine structure on the μ s time scale. However, this matches the known RC time response of the photodiodes and pre-amps, so it is this which is the likely cause rather than fine structure in the flash itself. The second feature was a rise in signal strength some 40 – 45 μ s after the impact on the Kapton. When combined with the projectile speed, these times did not match the distance to any structure in the target. Furthermore, it was not observed

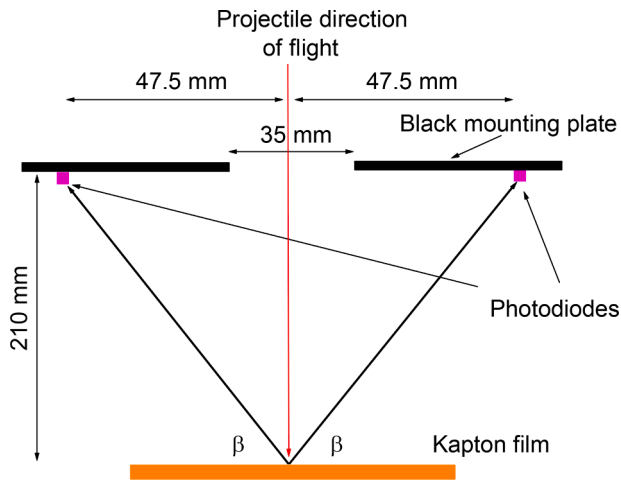


Fig. 5. Top-down view of a Kapton layer with a mounting plate in front of it with a central hole and two photodiodes looking at the Kapton. The red line shows the projectile direction. The line of sight from the impact site on the Kapton to the photodiodes is indicated, at an equal viewing angle β .

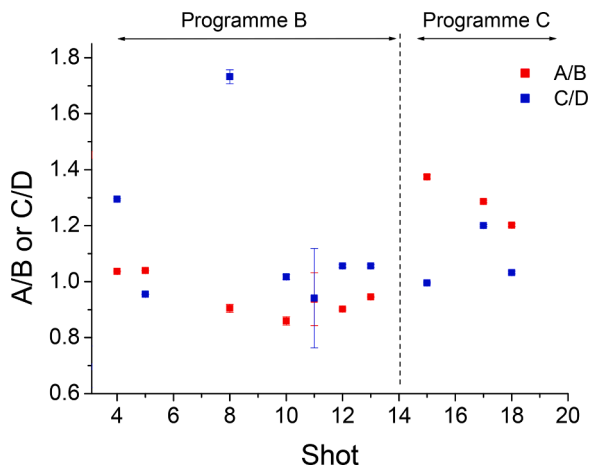


Fig. 6. Ratio of flash intensity for each pair of photodiodes A/B and C/D inside each shot in programmes B and C. If each photodiode in a pair, observed the same flash with the same sensitivity, the ratios should all equal 1. The large error bars on shot 11 reflect the low absolute magnitude of the signals in that shot.

in the earlier shots – it is therefore unexplained.

3. Results

3.1. Hole size

The holes made in the Kapton films by passage of the projectiles were circular to a high degree, with a rim around the hole, which mostly bent inwards as seen from the front, and outwards as seen from the rear. Example holes are shown in Fig. 4. The hole sizes were measured to within $\pm 1\%$ in all shots, except shots 1 – 3 and 15 where the film was damaged and torn and had to be replaced before measurements were made. The hole diameters track the projectile diameters to within the uncertainties (1 – 2%) over the full range of projectile diameters (i.e. f/d of 1/8 to 1/80). For 12.5 μm thickness of Kapton this has been previously reported by [50] for an $f/d = 1/80$ in a single layer of Kapton. However, [50], also observed that, for 1 mm diameter projectiles, the hole diameter in the second Kapton layer in a dual layer target was a few % larger than in the first layer. This was not observed here, although the

projectiles used here in the dual layer target were 0.3 – 0.8 mm diameter (i.e. smaller than in [50]).

3.2. Flash intensity

The light flash intensities in each of the 13 good shots are given in Table 2. A typical signal is shown in Fig. 3a for shot 8. Shot 8 featured two layers of Kapton, with 2 photodiodes (A and B) looking at the front of the first layer, and two (C and D) looking at the front of the second layer. The peak intensity is taken as the difference between the peak height and the pre-flash baseline level, with the uncertainties being due to the intrinsic noise in the system. Where (in programme B) there has been a contribution from the flash on Kapton layer 1 in the signals observed on layer 2 (as seen in Fig. 3a), this has been subtracted from the data, and the intensity given for C and D thus represents that from the impact on layer 2 alone.

3.2.1. Programme A

The data from photodiodes A and B in shot 1 (which were looking at the front of the Kapton layer) were found to have saturated. Attempts to exclude the saturated region and fit the remaining data to obtain an estimate of the peak failed, due to the large degree of saturation. Thus the data for shot 1 were not used in the intensity analysis.

Although data were obtained for the intensities on photodiodes A and B in shots 2 and 3, it was realised that in these shots there were also strong signals on photodiodes C and D which faced sideways and which were shielded from a direct line of sight to the Kapton film. These signals arose from reflections off the sidewalls in the chamber. Given that the reflected signal strength was significant, the contribution from the reflections to the signals on A and B is thus considered unknown, so no quantitative analysis was undertaken.

However, the results of programme A did reveal that the photodiodes could observe flash signals, and that the t_0 identification (i.e. the moment a light flash signal exceeds the noise threshold) was possible to within 1 μs . It was also concluded that signals from impacts of 1 mm st at 5 km s^{-1} would saturate the photodiode signals, so this combination was avoided in later shots. Finally it was decided to surround the sides of the targets with a blackout curtain in the subsequent programmes, to suppress reflections off the side walls of the chamber.

3.2.2. Programme B

This programme featured the dual-layer target (Fig. 2). During the analysis, a detailed inspection of the signal shapes in shot 4, revealed that the signals in photodiodes A and B (i.e., those looking at the front of the Kapton layer) were on the border of saturation. Attempts were made to reconstruct the signal shape and thus estimate the peak signal, by fitting the data (with the saturated region excluded) by a 3rd order polynomial. As a test, this was also done with the data from shot 5. Here the peak intensity found from the 3rd order polynomial fit with the peak data region excluded as in shot 4, gave a predicted peak intensity which differed by +3.7% from the actual observed value. This suggests the method gave a reliable estimate of the peak intensity, so the extrapolated results for shot 4 are provided in Table 2, with an uncertainty given by the extrapolation method accuracy.

The first step in the intensity analysis was to determine the relative sensitivity of the photodiodes given that there was no absolute calibration of each sensor. In all shots, the photodiodes pointing at the Kapton observed the impact point of the projectile as shown geometrically in Fig. 5, i.e. at a constant viewing angle β (77°). In programme C, the second layer of photodiodes observe the rear of the Kapton film in a mirror image of the set-up in Fig. 5. Given the characteristics of the photodiodes, this angle of incidence on the photodiode (13° from normal) should be within the 100% sensitivity region.

If, the projectile is indeed on the predicted central line of flight, all photodiodes have similar response functions, the pre-amps are all identical, and the impact plume is symmetrical, then, in any given shot,

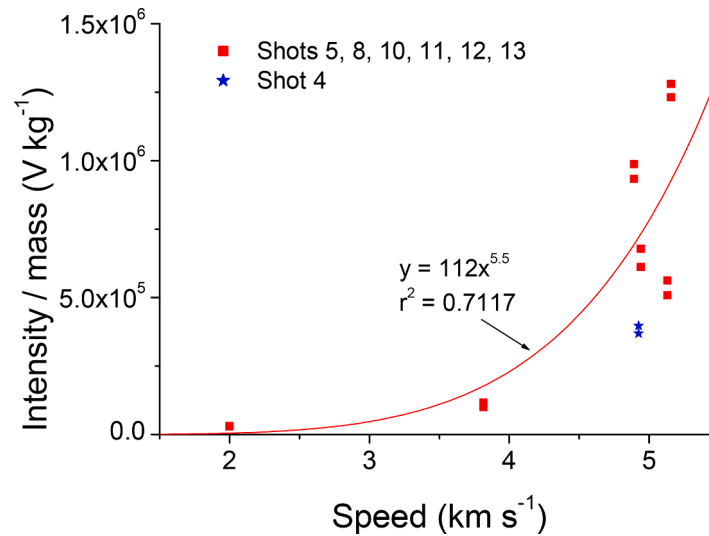


Fig. 7. Variation of flash intensity/projectile mass vs. impact speed for each photodiode looking at the front of the Kapton layers in programme B (with shot 4 shown as blue stars and excluded from the fit). There are two values for each shot (i.e. from photodiodes A and B). The fit was of the form $y = ax^p$.

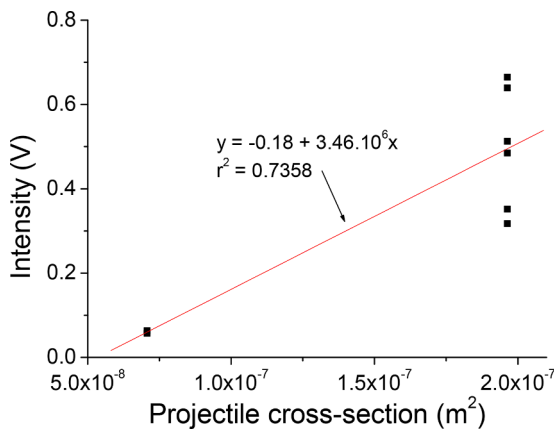


Fig. 8. Variation of flash intensity vs. projectile cross-section for each photodiode looking at the front of the first Kapton layer in shots 5, 8, 12 and 13 (i.e. at fixed speed of $\sim 5 \text{ km s}^{-1}$). A linear fit is shown.

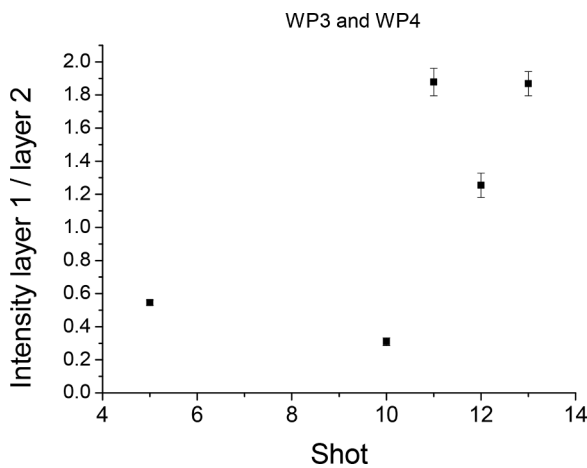


Fig. 9. Ratio of average layer 1 flash to the average layer 2 intensity in programme B. No clear trend is observed.

the peak signal amplitude on each pair of photodiodes (A and B, and C and D) should be equal. This is tested in Fig. 6, where the ratios A/B and C/D are shown for each shot. In programme B, the data in Fig. 6 mostly cluster around unity, with a mean of 0.97 ± 0.07 . This excludes the C/D ratios in shots 4 and 8, which were noticeably > 1 . The data for shot 8 for example, are shown in Fig. 3a, and the intensity of C clearly greatly exceeds that of D. No explanation was found for this.

The data in Fig. 6 for programme C show more scatter, ranging from 1.0 to 1.4. This appears to arise from the sampling issue due to the RC time constant identified earlier, and sets a limit on comparisons of data for the intensity in programme C.

It was reported by [28] that flash intensity normalised to projectile mass, scaled with impact speed to some power. Therefore in Fig. 7, the intensities (I) normalised to projectile mass (m) observed by photodiodes A and B in the shots in programme B are plotted vs. impact speed as measured by the gun (v). The values from shot 4 are excluded from the fit as they were extrapolated rather than measured. The result was:

$$I/m = (112 \pm 510) \times v^{(5.5 \pm 2.7)}, r^2 = 0.7117, \tag{1}$$

where intensity was in volts, mass in kg and speed in km s^{-1} . The associated goodness of fit criteria (the r^2 value) indicates the fit was reasonable even though the uncertainties on the coefficients in the fit are relatively large. As a comparison, the extrapolated values from shot 4 are also shown in Fig. 7, and lie slightly below the fit curve, indicating that the extrapolation may be underestimating the true peak values.

However, this form of the fit assumes that flash from a thin film is behaving similarly to the flash from impact on a semi-infinite target. An alternative hypothesis is that instead of scaling with projectile mass, at a fixed speed the intensity depends on the area of the hole in the Kapton. This could be because it depends on the amount and properties of the target material vaporised in the impact, rather than being determined by some function of the projectile's energy or momentum. Since it was shown previously by [50], and confirmed here (see Section 3.4) that the hole size in the Kapton has the same diameter as the projectile to within a few percent, we take the projectile cross-section as the hole size. This hypothesis can be tested using shots 5, 8, 12 and 13 where the speed was constant ($\sim 5 \text{ km s}^{-1}$) whilst projectile diameter varied from 0.3 to 0.5 mm. Accordingly, the intensity (I) in these shots is plotted vs. projectile cross-section (A) in Fig. 8. The data in Fig. 8 are fit with a linear function which yielded:

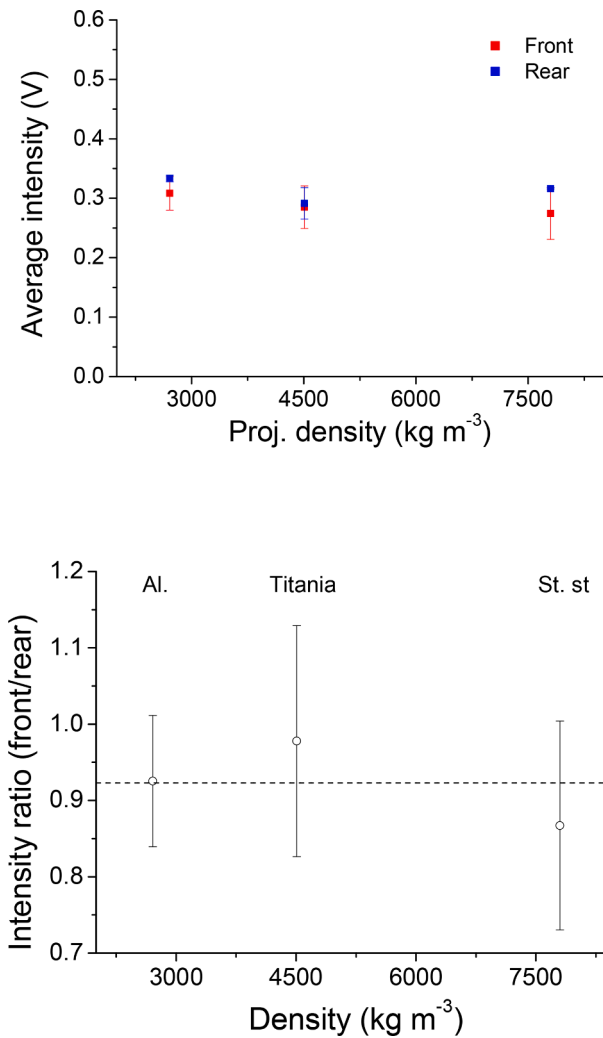


Fig. 10. Programme C. (a) The average intensity on the front face (average of A & B) and rear face (average of C & D). Despite the difference in projectile density (and hence mass), the intensities are all similar despite the results of programme B which suggested scaling with mass. (b) The ratio of the average flash intensity seen on the front face to that on the rear face. In all three cases, the rear face had a slightly greater intensity, but in each case this is within 1 sigma uncertainty of being equal.

Table 3

Speeds obtained from the light flash analysis compared to the measured gun speeds. Δt is the time between the two Kapton layers. The “Difference” (right-hand columns) is defined as (gun – flash) speed. The uncertainty in the flight flash speed comes from the uncertainty in the time interval between layers combined with the accuracy of the layer separation. The gun speed uncertainty is $\pm 1\%$.

Shot	Δt (μs)	Light flash speed (km s ⁻¹)	Gun speed (km s ⁻¹)	Difference	
				km s ⁻¹	%
4	113	4.912 \pm 0.032	4.925	0.013	0.26
5	108	5.139 \pm 0.035	5.157	0.018	0.33
8	109	5.091 \pm 0.034	5.131	0.040	0.78
10	145	3.827 \pm 0.020	3.816	-0.011	-0.29
11	284	1.954 \pm 0.010	2.000	0.046	2.3
12	112	4.955 \pm 0.033	4.943	-0.012	-0.24
13	113	4.912 \pm 0.032	4.892	-0.020	-0.41

$$I = -(0.18 \pm 0.15) + (3.46 \pm 0.85) \times 10^6 A, r^2 = 0.7358, \quad (2)$$

where I is in volts, A in m^2 and r^2 is the regression coefficient squared. The result is indeed consistent with a linear relation between flash intensity and hole area, although given the scatter on the data more experiments are needed to confirm this (see Programme C below).

The intensities from photodiodes C and D were not fit, as from Fig. 6 the data appeared more scattered than for A and B. However, the average intensity on Kapton layer 1 is compared to the average on layer 2 in Fig. 9 (excluding shot 4). As can be seen in Fig. 9, there is no general trend; in three of the shots the flash from layer 1 has a greater intensity than that from layer 2, but in two shots the reverse is true. It is not clear if this represents some variability in the response of each pair of photodiodes (A and B vs. C and D) which is greater than that between members of each pair, or if some other factor is responsible.

3.2.3. Programme C

Given that the nature of the signals changed between programmes B and C, it is not possible to directly compare the light intensities between these two programmes. However, we can compare the intensities between shots inside programme C. This is done in Fig. 10a, where the flash intensity is shown vs. projectile density (note that projectile diameter was a constant 0.5 mm, and impact speed was $\sim 4 \text{ km s}^{-1}$ in each shot). The data in Fig. 10a appear to have a flash intensity independent of projectile density. Given that all three shots have the same projectile diameter (1 mm) and equal speed ($\sim 4 \text{ km s}^{-1}$), this again suggests that the flash intensity is independent of projectile mass (and thus momentum or kinetic energy) and scales with projectile cross-section (i.e., with the area of the hole in the Kapton and thus with target, rather than projectile properties).

In Fig. 10b, the average intensity on the front face of the Kapton film (average of photodiodes A and B) is shown vs. that on the rear face (average of photodiodes C and D). The data appear close to unity, with the mean value across all three shots of 0.923 ± 0.055 , i.e. the uncertainty in the mean is less than the scatter in the data. This suggests that, within the uncertainties in the experiments, the flash intensity is the same when seen from the front or rear of the Kapton film.

3.3. TOF speed

The TOF data from programme 2 are given in Table 3. The TOF (Δt) is that between the start of the light flash in each layer. Given that the flash t_0 , in each layer of Kapton, can usually be identified to within a single data-bin, the error on each individual time is typically $\pm 0.5 \mu s$, and thus the error on Δt (called dt) is $0.71 \mu s$ in most cases. However, in shot 11 the signal amplitude is very small, and this led to a larger uncertainty in time of $1.4 \mu s$. The TOF speed was obtained from the layer separation d ($555 \pm 1 \text{ mm}$) divided by Δt . The uncertainty in the resultant speed is dominated by the uncertainty in the time (which is typically 0.6% compared to the 0.18% uncertainty in the distance). The % uncertainty in speed is shown vs. speed in Fig 11a, where the data are modelled by assuming that $dt = 0.71 \mu s$, layer separation (d) is 555 mm (where the error in the layer separation (Δd) is 1 mm), and by treating all errors as independent. The resulting prediction is shown (solid line) vs. speed in Fig. 11a, and is extrapolated to 20 km s^{-1} . From this prediction, it can be seen that for typical orbital debris impact speeds ($7 - 10 \text{ km s}^{-1}$) the predicted uncertainty in the measured speed is still less than 1%, and that even at higher speeds (15 km s^{-1}) typical of cosmic dust arriving from interplanetary space, the uncertainty is still only of order 2%.

Given that the timing uncertainty is a property of the photodiodes, the key design feature that can be easily varied is the layer separation. This is done in Fig. 11b, where the simple model used in Fig. 11a is adjusted for a range of layer separations d . For example, the SDS detector flown in 2019 had a d value of 150 mm for example. Using the light flash to determine the speed, and a Kapton layer thickness of 12.5

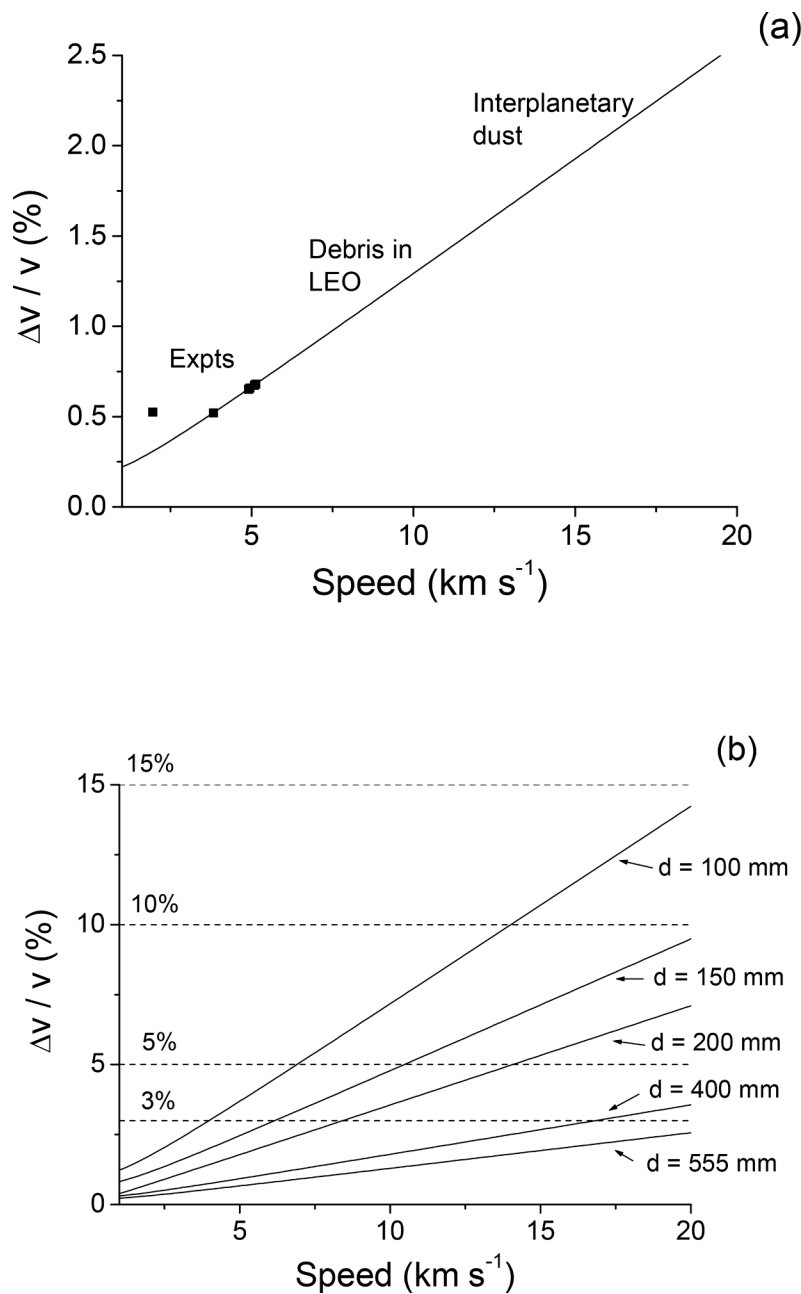


Fig. 11. The % uncertainty in the measured speed vs. speed. (a) The measured data are shown as black squares, and the solid line is the prediction based on a timing uncertainty of $0.71 \mu\text{s}$, a layer separation d , of 555 mm and an uncertainty in d of 1 mm. At the lowest speed, the datum shown is slightly above the predicted curve as the timing uncertainty in that case was $1.4 \mu\text{s}$. The mean speeds of debris in LEO and of interplanetary dust are shown, although it should be noted the actual speeds cover a wide range. (b) A range of predictions are given for the % uncertainty in the speed for various values of the layer separation d .

μm as used here, this gives a predicted speed uncertainty of just over 3% at speeds of 7 km s^{-1} , compared to the 18% reported for acoustic measurements of the TOF with SDS at that speed [44].

The speed in each shot obtained from the light flash signals is compared in Fig. 12, to those from the gun's normal speed measurement system. This is for shots at similar speed ($\sim 5 \text{ km s}^{-1}$) but where the projectile size varied and f/d ranged from $1/24$ (at 0.3 mm diameter) to $1/64$ (at 0.8 mm diameter). In Fig. 12, the data are shown as the ratio (gun speed) / (flash speed). If the two values are similar the ratio should be one. A simple average of the data gives a mean of (0.9985 ± 0.0048) , i. e. agrees with unity within errors, indicating no measureable deceleration as a result of passage through the Kapton layer at 5 km s^{-1} .

Fig. 13 shows the gun speed vs. the flash speed, for a fixed particle size (0.5 mm diameter) at varying speed. A fit to the data yielded a

perfect fit to a straight line with $y = x$, and this line is shown in Fig. 13, where the ratio (gun speed) / (flash speed) gives an average value of (0.9966 ± 0.0113) , again compatible with unity within the error.

3.4. Flash signal on PVDF acoustic sensor

In programme B, three PVDF sensors were mounted on the second Kapton film. One was on the front face (FK), one the rear face (RK) and one on the rear of the frame (RF). Unfortunately, PVDF sensor RK started to progressively fail (from shot 5 onwards), and gave a reduced signal for the acoustic vibrations. An example of the PVDF outputs is given in Fig. 14 for shot 4 where all three PVDF sensors still gave full responses to test stimuli. In Fig. 14, it can be seen that the FK and RK PVDF sensors show a signal at t_1 (when the impact on that layer of Kapton occurs) but

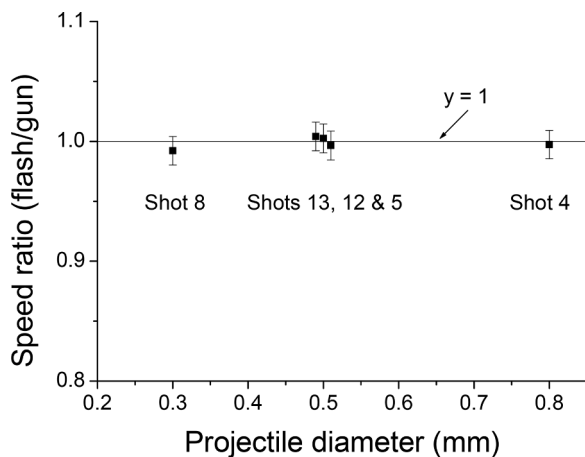


Fig. 12. Ratio of flash/gun speed vs. projectile diameter at fixed speed ($\sim 5 \text{ km s}^{-1}$). There are three data points at diameter = 0.5, so they have been off-set slightly along the x-axis for clarity. If the two speed measurements agree, the ratio should = 1 (this line is shown). No significant difference from unity is observed, indicating no deceleration due to passage through a single Kapton layer at 5 km s^{-1} .

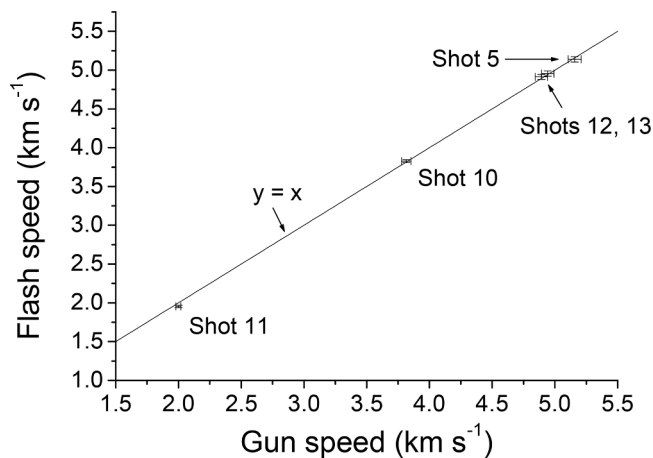


Fig. 13. Results for gun speed vs. photodiode (flash) speed (using only data for 0.5 mm diameter projectiles, i.e. $f/d = 1/40$). The line of $y = x$ is shown as a comparison.

that the expected acoustic signals start slightly later. This initial signal is taken as some form of EM pick-up from the pulse associated with the flash. It is a broader peak than the acoustic vibration peaks, and, when relaxing to the baseline level can overshoot before relaxing to the original level. Given that this signal is not seen on the PVDF sensor attached to the mounting frame, it appears to travel across the Kapton surface and not through free space. In shot 4, the signal was stronger on the front of the Kapton than the rear.

Of the seven shots in programme B, five showed an EM “pick-up” signal on PVDF sensor FK (which performed well throughout the programme) and two of these five (shots 4 and 5) also showed a signal on RK. Given that RK was failing, the lack of a “pick-up” signal in later shots is not necessarily significant. Of the 5 good signals on sensor FK, four start with a +ve going oscillation, and one with an initially -ve signal. The two shots without pickup signals (shots 8 and 12) were both at 5 km s^{-1} , so this is not related to impact speed as several shots at that speed did exhibit signals.

3.5. Acoustic wave speed in Kapton

Given the timing of the flash, and the acoustic vibration signals it should be possible to use the difference to calculate the speed of the acoustic transmission in the Kapton, if the distance from the hole to the sensor is known. Unfortunately, because one of the PVDF sensors on the Kapton (sensor RK) showed signs of failing from shot 5 onwards, the transmission times to the start of the signal are suspect in the later shots. However, in shot 4, the transmission time between impact flash t_0 and the start of the acoustic signal on the PVDF sensors was $31 \mu\text{s}$ for FK and $49 \mu\text{s}$ for RK. The hole in the Kapton film was measured to be 6.1 and 9.4 cm from FK and RK respectively. The uncertainty in time was $\pm 1 \mu\text{s}$, and in distance was $\pm 1 \text{ mm}$. This gives the calculated Kapton acoustic vibration transmission speed as $1968 \pm 71 \text{ m s}^{-1}$ (FK) and $1918 \pm 44 \text{ m s}^{-1}$ (RK). The speed reported in previous work on $12.5 \mu\text{m}$ Kapton films using just acoustic (PVDF) signals and triangulation methods to determine the impact time, was $1898 \pm 35 \text{ m s}^{-1}$ [50], compatible with the results here.

4. Conclusions

The light flash from hypervelocity impacts on thin Kapton films has been successfully observed using off-the-shelf photodiodes. The intensity and start time of the flash were measured. The magnitude of the flash scales with impact speed in the form $I/m = \alpha v^\beta$, where $\beta = 5.5$. This is compatible with impacts on solid targets, where values of β in the range 1.5 - 6 are commonly reported at impact speeds of 1 - 6 km s^{-1} (e.g. see [4] for a review and Swift *et al.*, 2011), although there are issues with this. For example, it has previously been pointed out that such a strong dependence on impact speed would fail when extrapolated to speeds above 10 km s^{-1} , because it implies that the fraction of the impact energy emitted as visible light would exceed unity as speed increased. Consequently, at higher speeds the dependence has to be less, or even minimal (Swift *et al.*, 2011). Additionally, as pointed out by [29]) the light flash intensity depends on the ambient pressure in the target chamber, and it is not clear if this also influences β .

Nevertheless, we note several points regarding impact flash intensity from the present study. The first is that the scaling applies even though the target films were very thin (with f/d ratio of $1/8$ to $1/80$), and there is no appreciable loss of projectile energy during the impact (the projectile neither slows down nor changes size, i.e. does not lose mass, during passage through the thin film). Secondly, the data support the hypothesis that the absolute flash intensity at a given speed depends on the area of the hole made in the Kapton (which is essentially the projectile cross-sectional area in the thin film), rather than with projectile mass. Further, the intensity of the flash as observed on the front and rear of the film being hit, appears the same (within uncertainties).

The good time resolution for the determination of the start of the detectable light flash signals permits time resolution on the time of flight between two Kapton layers to typically slightly better than $1 \mu\text{s}$. This, combined with good signal/noise levels, allows the transit time between two Kapton layers to be sufficiently accurately determined that the speed of the projectile can be found to typically $\pm 0.7\%$, even at speeds of 5 km s^{-1} . The physical separation of the layers can be found to $\pm 1 \text{ mm}$, suggesting that the separation could be reduced to of order 150 mm with just 10% resulting uncertainty on the speed determination.

It was found that at speeds of 2 - 5 km s^{-1} , no projectile deceleration was observed in the range of f/d of $1/24$ - $1/64$. Indeed, for 0.3 mm projectiles no deceleration was observed at speeds of 5 km s^{-1} , and even at 2 km s^{-1} no deceleration was observed for a 0.5 mm projectile. Future work to reduce the minimum projectile size (and hence extend the f/d range) and to determine the lower speed at which flash can be observed, would be beneficial.

The impact light flash event is also shown to produce signals on nearby PVDF acoustic sensors. These appear to couple to the EM pulse via the Kapton film. This confirms the suspicions in past work, with real

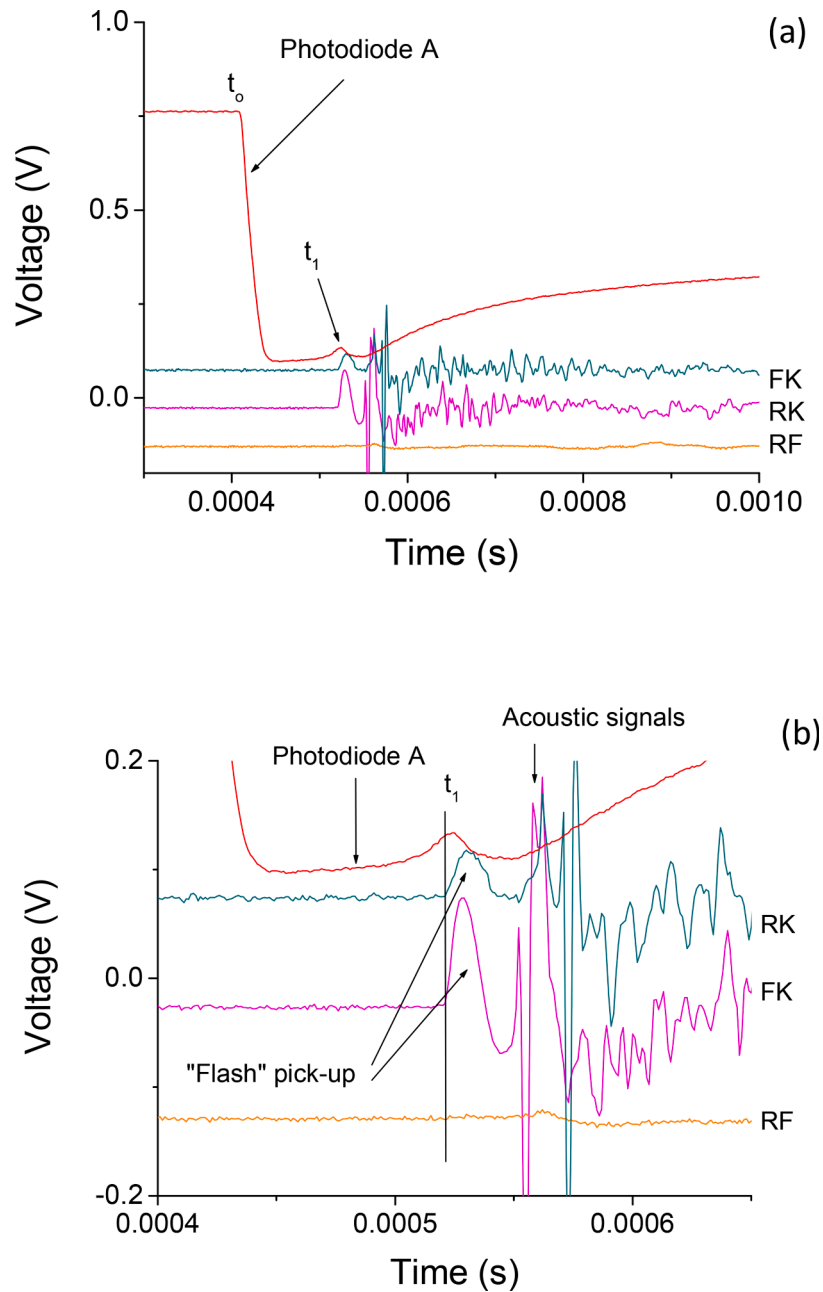


Fig. 14. (a) Acoustic PVDF signals in shot 4. At t_0 (the impact time on the first Kapton layer) no signals occur on the PVDF sensors (which are on the second Kapton layer). Then at t_1 , which can be taken from when the photodiode signal A starts to rise again, there is a “pick-up” signal on both the PVDF sensors on the second Kapton layer (RK and FK) but not from the sensor on the frame (RF). (b) The same data are shown on expanded axes. FK and RK show signals that start coincident with t_1 to within one time increment (1 μ s) and which has a longer period than the expected acoustic vibration signals (marked with an arrow). There is a slight response from RF accompanying the acoustic signals on RK and FK but it is very weak. (Note that to avoid overlapping data, RK and RF are offset by +0.1 and -0.1 V respectively).

data from the SDS impact detector flown in space in 2019, [49] and in previous laboratory experiments [50]. The characterisation of this signal in the present work, will enable it to be recognised within real data from PVDF sensors and allowed for during analysis. Indeed, if light flash (photodiode) data were combined with acoustic (PVDF) data, a more powerful dust impact detector can be envisaged which has accurate timing, and can provide impactor speed and direction (using triangulation of the acoustic signals on a layer of Kapton) to a high precision.

The experiments reported herein are for normal incidence impacts on a simple prototype detector. A real space deployed instrument would need further developments. For example, in space impacts will not all be at normal incidence, unless some streaming effect is present (see [53],

for a discussion on oblique impacts in space). Here, the detector requires a finite depth to have two well separated layers, and, given a finite exposed surface area this implies a limited field of view, the NASA SDS detector for example envisaged detecting impacts through both layers at up to 30° from normal incidence. Thus, it would be sensible to test the light flash response over such a range of inclinations. In addition, a sealed unit should also be tested, such that the photo-diodes are internal and not exposed to external light sources (such as the sun, Earth-light, Moon-light, local light sources on the hosting spacecraft, etc.). To help reduce ambient light levels in the interior of such a detector, the front Kapton film could also be coated with a thin layer of an opaque coating, such as palladium (see [54]). This would also have the benefit of

reducing erosive effects due to atomic oxygen in LEO for example. Modelling of the impact flash and extrapolation to higher impact speeds than achievable in a light gas gun would also be desirable.

As stated above, an ideal detector would need to locate the impact holes on both layers in order to get the flight trajectory of the impactor. This is not only necessary to get the track length between the two layers, but, when combined with the measured speed, provides the data necessary to predict the orbit of the impactor (provided the pointing history of the detector is known). The current light flash method does not provide this information. However, by using PVDF acoustic sensors on both layers, it is possible to obtain the necessary data (plus a resistive grid on the front layer for hole size). Thus a flight model would use a mixture of light flash and acoustic detectors to provide impact speed, direction and size for the incident particle.

Taken together, the results presented here suggest that TOF speed measurement systems using 12.5 μm Kapton films, would potentially be ideal for use in cosmic dust and space debris detectors in LEO, where speeds will have an average of a few km s^{-1} (debris) up to mean values of 15 - 20 km s^{-1} (interplanetary dust). Higher impact speeds are also possible (e.g. from some cometary dust grains or interstellar dust which can penetrate into the inner solar system).

CRedit authorship contribution statement

L.S. Alesbrook: Conceptualization, Data curation, Investigation, Methodology, Writing – review & editing. **M.J. Burchell:** Conceptualization, Funding acquisition, Investigation, Methodology, Supervision, Writing – original draft, Writing – review & editing. **L.T. Cornwell:** Investigation, Methodology, Writing – review & editing. **R.D. Corsaro:** Conceptualization, Funding acquisition, Methodology, Writing – review & editing. **F. Giovane:** Conceptualization, Methodology, Writing – review & editing. **J.-C. Liou:** Funding acquisition, Writing – review & editing. **J. Tandy:** Investigation, Methodology, Writing – review & editing. **P.J. Wozniakiewicz:** Funding acquisition, Supervision, Writing – review & editing.

Declaration of competing interest

The authors declare the following financial interests/personal relationships which may be considered as potential competing interests: Burchell reports financial support was provided by Astroacoustics. Cornwell reports financial support was provided by GNOSIS (STFC). If there are other authors, they declare that they have no known competing financial interests or personal relationships that could have appeared to influence the work reported in this paper.

Data availability

Data will be made available on request.

Acknowledgements

The Authors wish to thank Astroacoustics (US) for a grant to support this work. LTC was supported by the University of Kent and the UK Global Network On Sustainability In Space (GNOSIS) (GNOSIS Network - Solving the growing space debris problem) which is funded by a grant from STFC (the Science and Technology Facilities Council, UK).

References

- [1] Melosh HJ. Contact and compression stage of impact cratering. In: Osinski GR, Pierazzo E, editors. *Impact cratering processes and products*. Wiley-Blackwell; 2013. p. 32–42. ISBN 978-1-4051-9829-5.
- [2] Atkins WW. Flash associated with high velocity impact on aluminum. *J Appl Phys* 1955;26:126–7.

- [3] Gehring J, Warnica R. Investigation of the reaction of the lunar surface to the impact of a lunar probe. Final Report for Contract Grant JPL-950299. Jet propulsion laboratory. California Inst. of Tech.; 1963. <https://ntrs.nasa.gov/ap/i/citations/19650021459/downloads/19650021459.pdf>.
- [4] Burchell MJ, Robin-Williams R, Foing BH. The SMART-1 lunar impact. *Icarus* 2010; 207:28–38.
- [5] Burchell MJ, Cole MJ, Ramkissoon NK, Wozniakiewicz PJ, Price MC, Foing B. Smart-1 end of life shallow regolith impact simulations. *Meteorit Planet Sci* 2015; 50:1436–48. <https://doi.org/10.1111/maps.12479>.
- [6] Ehrenfreund P, Foing BH, Veillet C, Wooden D, Gurvits L, Cook AC, Koschny D, Biver N, Buckley D, Ortiz JL, Di Martino M, Dantowitz R, Cooke B, Reddy V, Wood M, Vennes S, Albert L, Sugita S, Kasuga T, Meech K, Tokunaga A, Lucey P, Krots A, Palle E, Montanes P, Trigo-Rodriguez J, Cremonese G, Barbieri C, Ferri F, Mangano V, Bhandari N, Chandrasekhar T, Kawano N, Matsumoto K, Taylor C, Hanslmeier A, Vaubaillon J, Schultz R, Erd C, Gondoin P, Levasseur-Regourd AC, Khodachenko M, Rucker H, Burchell M, Cole M, Svedhem H, Rossi A, Colaprete T, Goldstein D, Schultz PH, Alkalai L, Banerdt B, Kato M, Graham F, Ball A, Taylor E, Baldwin E, Berezchnoy A, Lammer H, Talevi M, Landeau Constantin JV, Weyhe B, Ansari A, Lawton C, Lebreton JP, Friedman L, Betts B, Buoso M, Williams S, Cirou A, David L, Sanguy O, Burke JD, Maley PD, deMoraes VM, Marchis F, Munoz JHM, Dighaye J-L. SMART-1 impact ground-based campaign. In: 38th lunar and planetary science conference; 2007. abstract #2446.
- [7] Veillet C, Foing B. SMART-1 impact observation at the Canada–France–Hawaii telescope. In: 38th lunar and planetary science conference abstract 1520; 2007.
- [8] Ortiz J, et al. Optical detection of meteoroidal impacts on the Moon. *Nature* 2000; 405(6789):921–3.
- [9] Oberst J, Christou A, Suggs R, Moser D, Daubar LJ, McEwen AS, Burchell M, Kawamura T, Hiesinger H, Wünnemann K, Wagner R, Robinson MS. The present-day flux of large meteoroids on the lunar surface - a synthesis of models and observational techniques. *Planet Space Sci* 2012;74(1):179–93. <https://doi.org/10.1016/j.pss.2012.10.005>.
- [10] Ortiz JL, Aceituno FJ, Quesada JA, Aceituno J, Fernandez M, Santos-Sanz P, Trigo-Rodriguez JM, Llorca J, Martin-Torres FJ, Montanes-Rodriguez P, Palle E. Detection of sporadic impact flashes on the Moon: implications for the luminous efficiency of hypervelocity impacts and derived terrestrial impact rates. *Icarus* 2006;184:319–26.
- [11] Gores PAS, Spray JG. Hypervelocity impact of anorthosite: excavation, spallation and crater reconstruction. *Int J Impact Eng* 2022;160:104078.
- [12] Jean B, Rollins T. Radiation from hypervelocity impact generated plasma. *AIAA J* 1970;8(10):1742–8.
- [13] Swift, W.R., Moser, D.E., Suggs, R.M., Cooke, W.J. An exponential luminous efficiency model for hypervelocity impact into regolith. In: Cooke, W.J., Moser, D. E., Hardin, B.F., Janches, D., (Eds.) *Meteoroids: The Smallest Solar System Bodies*, Proceedings of the Meteoroids Conference held in Breckenridge, Colorado, USA, May 24–28, 2010. NASA/CP-2011-216469, p. 125, 2011.
- [14] Mihaly JM, et al. Pressure-Dependent, Infrared-Emitting Phenomenon in Hypervelocity Impact. *J Appl Mech* 2015;82:011004. -1.
- [15] Simpson G, Moreno J, Schaeffer M, Ramesh KT. First contact: fine structure of the impact flash and Ejecta during hypervelocity impact. *PNAS Nexus* 2023;2:1–14. <https://doi.org/10.1093/pnasnexus/pgad214>.
- [16] Tandy JD, Price MC, Wozniakiewicz PJ, Cole MC, Alesbrook LS, Avdellidou C. Impact flash evolution of CO₂ ice, water ice, and frozen Martian and lunar regolith simulant targets. *Meteorit Planet Sci* 2020;55(10):2301–19.
- [17] Tsemelbis K, Burchell MJ, Cole MJ, Margaritis N. Residual temperature measurements of light flash under hypervelocity impact. *Int J Impact Eng* 2008;35: 1368–73.
- [18] Lawrence RJ, Reinhardt WD, Chhabildas LC, Thornhill TF. Spectral measurements of hypervelocity impact flash. *Int. J. Impact Engng* 2006;33:353–63.
- [19] Sugita S, Schultz PH. Interactions between impact-induced vapor clouds and the ambient atmosphere: 1. Spectroscopic observations using diatomic molecular emission. *J Geophys Res* 2003;108:5051.
- [20] Sugita S, Schultz PH. Interactions between impact-induced vapor clouds and the ambient atmosphere: 2. Theoretical modelling. *J Geophys Res* 2003;108:5052.
- [21] Sugita S, Schultz PH. Spectroscopic characterization of hypervelocity jetting: comparison with a standard theory. *J Geophys Res* 1999;104:30825–45.
- [22] Sugita S, Schultz PH, Adams MA. Spectroscopic measurement of vapor clouds due to oblique impacts. *J Geophys Res* 1998;103:19427–41.
- [23] Sugita S, Schultz PH, Hasegawa S. Intensities of atomic and molecular bands observed in impact-induced luminescence. *J Geophys Res* 2003;108:5140.
- [24] Tandy JD, Mihaly JM, Adams MA, Rosakis AJ. Examining the temporal evolution of hypervelocity impact phenomena via high-speed imaging and ultraviolet-visible emission spectroscopy. *J Appl Phys* 2014;116:034901.
- [25] Verreault J, Day JPR, Halswijk WHC, Loiseau J, Huneault J, Higgins AJ, Devir AD. Emission spectroscopy of hypervelocity impacts on aluminum, organic and high-explosive targets. *Procedia Eng* 2015;103:618–27.
- [26] Yafei H, Enling T, Liping H, Meng W, Kai G, Jin X, Jianjun M, Shuhua L, Ruizhi W, Zhenbo L. Evolutionary characteristics of thermal radiation induced by 2A12 aluminum plate under hypervelocity impact loading. *Int J Impact Eng* 2019;125: 173–9.
- [27] Burchell MJ, Kay L, Ratcliff PR. Use of combined light flash and plasma measurements to study hypervelocity impact processes. *Adv Space Res* 1996;17: 141–5.
- [28] Eichhorn G. Analysis of the hypervelocity impact process from impact flash measurements. *Planet Space Sci* 1976;24:771–81.
- [29] Eichhorn G. Measurements of the light flash produced by high velocity particle impact. *Planet Space Sci* 1975;23(11):1519–25.

- [30] Burchell MJ, Cole MJ, Ratcliff PR. Light flash and ionization from hypervelocity impacts on ice. *Icarus* 1996;122:359–65.
- [31] Kissel J. The particulate impact analyzer, an instrument to analyze small particles released by Halley's Comet. In: Proceedings of the international meeting on the Giotto Mission, Noordwijkerhout. 169; 1981. p. 53–60. The Netherlands. ESA Spec. Publ.ESA-SP.
- [32] Kissel J, et al. Composition of comet Halley dust particles from Giotto observations. *Nature* 1986;321:336–7.
- [33] Wozniakiewicz P. Cosmic dust in space and on Earth. *Astron Geophys* 2017;58(1): 1.35–40. <https://doi.org/10.1093/astrogeo/atx027>.
- [34] Liou JC, Johnson NL. Risks in Space from orbiting Debris. *Science* (1979) 2006; 311:340–1. <https://doi.org/10.1016/j.asr.2005.06.021>.
- [35] Wozniakiewicz PJ, Burchell MJ. Space dust and debris near the Earth. *Astron Geophys* 2019;60(3):38–42. <https://doi.org/10.1093/astrogeo/atz150>.
- [36] Kessler D.J. Critical density of spacecraft in low earth orbit. NASA JSC-28949, NASA Johnson Space Center, Houston, TX, 2000. <https://aquarid.physics.uwo.ca/kessler/Critical%20Density-with%20Errata.pdf>.
- [37] Cowardin H, Anz-Meador P, Murray J, Liou JC, Christiansen E, Sorge M, Fitz-Coy N, Huynh T. Updates to the DebrisSat project in support of improving breakup models and orbital debris risk assessments. In: 2019 15th Hypervelocity Impact Symposium, HVIS; 2021. p. 572–80. <https://doi.org/10.1115/HVIS2019-066>.
- [38] Humes, D.H. Small craters on the meteoroid and space debris impact experiment. in *LDEF - 69 Months in space third post-retrieval symposium part 1* (ed. Levine, A. S.) 287–322 (NASA Conference Publication 3275, 1993).
- [39] Miao J, Stark JPW. Direct simulation of meteoroids and space debris flux on LDEF spacecraft surfaces. *Planet Space Sci* 2001;49:927–35.
- [40] Kearsley AT, et al. Impacts on Hubble Space Telescope solar arrays: discrimination between natural and man-made particles. *Adv Space Res* 2005;35:1254–62.
- [41] Kearsley AT, et al. The chemical composition of micrometeoroids impacting upon the solar arrays of the Hubble Space Telescope. *Adv Space Res* 2006;39:590–604. <https://doi.org/10.1016/j.asr.2006.05.011>.
- [42] Kearsley AT, et al. Hypervelocity impact in low earth orbit: finding subtle impactor signatures on the Hubble Space Telescope. *Procedia Eng* 2017;204:492–9. <https://doi.org/10.1016/j.proeng.2017.09.746>.
- [43] Corsaro RD, Giovane F, Liou J-C, Burchell MJ, Cole MJ, Williams EG, Lagakos N, Sadilek A, Anderson CR. Characterization of space dust using acoustic impact detection. *J Acoust Soc Am* 2016;140(2):1429–38. <https://doi.org/10.1121/1.4960782>.
- [44] Hamilton J, Liou J-C, Anz-Meador PD, Corsaro B, Giovane F, Matney M, Christiansen E. Development of the space debris sensor. In T. Schmitz & F. Flohrer (Eds.). In: 7th European conference on space debris; 2017. ESA Space Debris Office, <https://conference.sdo.esoc.esa.int/proceedings/sdc7/paper/965>.
- [45] Liou J-C, Corsaro R, Giovane F, Anderson C, Sadilek A, Burchell M, et al. DRAGONS – a micrometeoroid and orbital debris impact sensor. <https://ntrs.nasa.gov/archive/nasa/casi.ntrs.nasa.gov/20150019424.pdf>.
- [46] Burchell MJ, Standen S, Cole MJ, Corsaro RD, Giovane F, Liou J-C, Pisacane V, Stansbery E. Acoustic response of aluminum and Duroid plates to hypervelocity impacts. *Int J Impact Eng* 2011;38:426–33.
- [47] Burchell MJ, Corsaro R, Giovane F, Cole M, Sadilek A, Price MC, Liou JC. A new cosmic dust detector with a novel method using a resistive grid sensitive to hypervelocity impacts. *Procedia Eng* 2013;58:68–76. <https://doi.org/10.1016/j.proeng.2013.05.010>.
- [48] Faure P, Masuyama S, Nakamoto H, Akahoshi Y, Kitazawa Y, Koura T. Space dust impacts detector development for the evaluation of ejecta. *Procedia Eng* 2013;58: 594–600.
- [49] Anz-Meador, P., Ward, M., Manis, A., Nornoo, K., Dolan, B., Claunch, C., Rivera, J. The Space Debris Sensor Experiment. Presented at the First International Orbital Debris Conference, Texas (USA). 10 pages. 2019. URL: <https://ntrs.nasa.gov/citations/20190033909>.
- [50] Cornwell LT, Wozniakiewicz PJ, Burchell MJ, Alesbrook LA, Corsaro RD, Giovane F, Liou J-C. A study on the capabilities and accuracy of Kapton based TOF space dust and debris detector. *Adv Space Res* 2023;72:2959–70. <https://doi.org/10.1016/j.asr.2022.07.022>.
- [51] Burchell MJ, Cole MJ, McDonnell JAM, Zarnecki JC. Hypervelocity impact studies using the 2 MV Van de Graaff dust accelerator and two stage light gas gun of the University of Kent at Canterbury. *Meas. Sci. Tech.* 1999;10:41–50. <https://iopscience.iop.org/article/10.1088/0957-0233/10/1/011/pdf>.
- [52] Hibbert R, Cole MJ, Price MC, Burchell MJ. The hypervelocity impact facility at the University of Kent: recent upgrades and specialized capabilities. *Procedia Eng* 2017;204:208–14. <https://doi.org/10.1016/j.proeng.2017.09.775>.
- [53] Pierazzo E, Melosh HJ. Understanding oblique impacts from experiments, observations and modelling. *Ann Rev Earth Planet Sci* 2000;28:141–67.
- [54] Dignam A, Wozniakiewicz P, Burchell M, Alesbrook LS, Tighe A, Suliga A, Wessing J, Kearsley A, Bridges J, Holt J, Howie S, Peatman L, Fitzpatrick D. Palladium-coated Kapton for use on dust detectors in low Earth orbit: performance under hypervelocity impact and atomic oxygen exposure. *Front Space Technol* 2022;3:933664. <https://doi.org/10.3389/frspt.2022.933664>.